A perspective on the catalytic hydrogenation of aromatics by Co(Ni)MoS phases

Hervé Toulhoat

Version of Record: https://www.sciencedirect.com/science/article/pii/S0021951721000221
Manuscript_638662b485b1d1db2f17981bcabe2fe1

A perspective on the catalytic hydrogenation of aromatics by Co(Ni)MoS phases

Hervé Toulhoat [a,*1]

[a]IFP Energies nouvelles, 1 & 4 avenue de Bois-Préau, 92852 Rueil-Malmaison, France

*Correspondence to: herve.toulhoat@orange.fr

Abstract : Hydrogenation of aromatics by catalytic hydroprocessing is necessary in the upgrading of fossil hydrocarbons into fuels and bases for petrochemistry. In this paper the meaning and applicability are discussed of the "rim-edge" model, the outstanding hydrogenation activities of NiMoS supported on NiSx, and the effect of doping by the hard anion-forming elements phosphorous, boron, and fluorine.

Keywords: Hydrotreating Catalysts, NiMoS phase, Hydrogenation of Aromatics, Doping effects

Highlights:

- Rim-edge model challenged
- Doping by P, B, F has distinct effects on hydrogenation activity and acidity
- A "sulfhydrophobic" effect may explain the boosted hydrogenation by dopes

[1] Present address : Laboratoire de Réactivité de Surface, Sorbonne Université, CNRS, F-75005 Paris, France

1 Introduction

Elegant Mössbauer experiments by Henrik Topsøe et al. established that the active phase of optimal industrial CoMo hydrotreating catalysts is a mixed sulfide, which they termed the CoMoS phase [1]. This initiated a very rich stream of important research results until today, which in particular allowed to extend this discovery to analogous systems in which Co is substituted by Ni and Mo by W. Besides hydrodesulfurization (HDS), an important function of hydrotreating catalysts and processes in the refinery is to allow upgrading of heavy cuts in presence of sulfur and nitrogen compounds, by increasing the H/C ratio of products. This requires the activation of the hydrogenation of aromatic nuclei (HYD) by Co(Ni)Mo(W)S phases under hydroprocessing conditions. This transfer of molecular dihydrogen towards the slate of liquid refined fuels is key to improve their energetic value and combustion properties, as depicted by the Stangeland diagram [2] of Fig. 1. The present paper is focused on the identification of the optimal catalysts [3] for the hydrogenation of aromatics under hydroprocessing conditions, i.e. in the presence of H_2+H_2S sulfo-reducing mixtures. The optimal catalyst will be defined as the one presenting the highest stable turnover frequency (TOF) for the reaction aimed at, under given reaction conditions, and the optimally efficient catalyst as the one expressing the highest number of stable and working active sites per unit of reaction volume. The difference of definitions expresses the gap existing between a model catalyst, designed to experimentally measure a TOF as accurate as possible, and a practical catalyst, which is compliant with all chemical engineering rules, as well as manufacturing and economical constraints.

When catalytic activities per site (or TOFs) are plotted on the ordinate (usually on a log scale) against an appropriate numerical “descriptor” of the strength of interaction of a key reactant with catalytic sites for chemical series of analogous catalysts (e.g. solids that sample

periods of the Periodic Table), they often present a strong maximum. Such "Volcano curves" present experimental evidence of the validity of the Sabatier Principle [4]. This strength of interaction must be large enough to activate reactants but low enough to avoid poisoning of the sites. Famous early examples of volcano curves were presented using experimental descriptors such as estimates of adsorption strengths [5, 6]. But only recently modern first principles theoretical chemistry methods, coupled with the exponentially increasing numerical computing power, allowed to generalize the inventory of volcano curves described by computed binding strengths [7-9]. These methods simultaneously offered perspectives for "in silico discovery" of new optimal catalysts.

Recently a simple linear relationship was shown to exist between the optimal bond strength descriptor in a family of catalysts, and the enthalpy of the considered reaction [3]. A theory of this striking connection between kinetics and thermodynamics was developed. Among the set of 12 examples presented in support of this relationship [3], are volcano curves for thiophene HDS, and for the hydrogenation (HYD) of biphenyl HYD catalyzed by transition metal sulfides (TMS) under sulforeductive conditions. The interactions are described by E_{MS} a computed transition metal-sulfur bond strength in the bulk TMS representative of the key catalytic interaction. The E_{MS} descriptors of the Co(Ni)Mo(W)S phases were shown to obey simple lever rules combining descriptors of the parent binary sulfides (Co_9S_8, Ni_3S_2, MoS_2 and WS_2). It explains the empirical longstanding knowledge that CoMoS is closer to the optimal catalyst for HDS, and NiWS closer to the optimal catalyst for HYD. Catalyst rankings are actually CoMoS > NiMoS > NiWS > CoWS for HDS, and NiWS > NiMoS > CoMoS > CoWS for HYD [10-13]. Indeed, the about 20% lower enthalpy of HYD than of HDS, the latter involving saturation of a thio-aromatic hydrocarbon plus C-S bond hydrogenolysis leading to ring opening and H_2S production, determines an about 10% lower optimal E_{MS} for HYD. In view of the exponential sensitivity of TOFs to descriptor

values in the vicinity of volcano plot maxima, the selectivities of Co(Ni)Mo(W)S phases toward HYD and HDS are clearly distinct and this is implemented in industrial practice, whenever a compromise must be found between depth of HDS and cost of H_2 consumed, for a given target in the crude oil refining process.

The so called "Rim-Edge" model was introduced by Daage and Chianelli [14] in 1994 to explain their results in the HDS of dibenzothiophene (DBT) catalyzed by MoS_2 powders annealed under 15% H_2S + 85% H_2 gas flow between 350 and 900 °C. The size and morphology of the resulting crystallites were determined by XRD. A Debye-Scherrer analysis of the (002) peak-narrowing showed that the number of stacking layers of the MoS_2 sheets varied between N = 3 and 15 (the heights h increased from 2 to 9 nm) with increasing annealing temperature. Simultaneously, the diameter L along the basal plane did not vary much between L = 4 and 6 nm. Since the HDS of DBT occurs according to two concurrent pathways, DDS or Direct DeSulfurization producing primarily biphenyl (BP), and HYD or Hydrogenation pathway, producing the semi-hydrogenated primary intermediate tetrahydrodibenzothiophene (H4DBT), a kinetic analysis allowed these authors to evaluate rate constants for each step and each catalyst. They showed than the ratio of rate constants k_{H4DBT}/k_{BP}, a measure of the catalyst selectivity towards HYD over DDS, depends on the morphology. Since according to the CoMoS model and the geometrical model of Kasztelan et al. [10] active sites are situated on the edges of the MoS_2 sheets, and L hardly varied, Daage and Chianelli distinguished the terminal layer edges (which they called rims) and the intermediate layer edges (called edges) in the stacks and assigned HYD specific sites to rims only. From their structural data they computed rim densities (site.g^{-1}) and showed that k_{H4DBT} (molecule.g^{-1}.s^{-1}) is strictly proportional to rim densities, deducing a TON of about 0.003 molecule.$site^{-1}$.s^{-1} under the applied operating conditions (350 °C, 30 bar H_2). This result was

rationalized in terms of steric hindrance for site specific adsorption of a large molecule as DBT, rim sites being less hindered than edge sites.

This convincing and elegant study of the "pre-DFT era" became very popular, and triggered efforts to improve HYD selectivities of industrial supported catalysts by minimizing stacking. The outcomes were, however, not as convincing, maybe too constrained by interactions of the active phase with the supports. Moreover, a few years later DFT studies did not confirm that DBT and H4DBT chemisorb preferentially on rims, but showed that they can be stabilized also on edges in multi-point modes [15].

As discussed above, in terms of TOFs, NiWS is closer to the optimal catalyst for HYD in sulforeductive conditions, followed by NiMoS, but other considerations, including cost, determine a much wider range of applications for the latter. Besides, research efforts addressed several ways to optimize the efficiency of NiMoS. Among them, attempts to monitor sizes and morphologies of catalytic particles so as to maximize the active site densities, i.e. dispersion, were in the spirit of rational design. Other ways resulted from fortuitous discoveries, such as the doping effect of hard anion-forming elements fluorine, phosphorous, and boron, or NiSx as a support. In what follows, dispersion effects are discussed in the light of a simplified geometrical model in section 2, which covers the Rim-Edge model, the type I/type II concept, and to some extent the specificities of S-edges and M-edges. The support effect of NiSx on NiMoS morphologies is also examined in this section. In section 3, the origin of the doping effect by hard-anion forming elements is discussed, and a new unifying interpretation of this effect proposed.

2 Test of the Rim-Edge model with a simplified geometrical model

First, let us attempt to apply the Rim-Edge analysis to a few series of comparable catalysts, for which structural characterization as well as kinetic data have been published, in

order to check to which extent this concept can be generalized. For this purpose, either XRD or TEM characterizations will be exploited, since both may provide averages of the stacking number N and the particle diameter L.

Consider an average Co(Ni)MoS catalytic nanoparticle of MoS_2-like structure, made of a stack of N layers of basal diameter L. Omitting shape factors, the following simple equations hold for isolated unsupported nanoparticles:

$$V \sim NL^2 \qquad (1)$$

$$E \sim (N-2)L \qquad (2)$$

$$R \sim 2L \qquad (3)$$

where $\sim$ means "proportional to", V is the volume of the particle, E the length of its edges, and R is the length of its rims. Let us assume that for supported nanoparticles one of the two Rims is hindered by the support, so that equation (3) becomes:

$$R_S \sim L \qquad (4)$$

where R_S is the length of active rims for supported catalysts. Let us now compare catalysts with the same Mo content, C in $g.g^{-1}$. Let σ_i be the specific number of MoS_2-like catalytic nanoparticles (in g^{-1}) for catalyst i of density d_{MoS_2}. We then can derive:

$$C = \sigma_i V_i d_{MoS_2} \qquad (5)$$

So that from (1):

$$\sigma_i \sim \frac{C}{d_{MoS_2} N_i L_i^2} \qquad (6)$$

Assuming that HYD sites are located exclusively on the rims, and with μ_i the maximal density of active HYD sites (in $site.g^{-1}$), we have:

$$\mu_{iR} = \left(\frac{R_i}{l}\right)\sigma_i \qquad (7)$$

where l is the minimal distance on a rim or an edge between active sites, assumed to be determined by the MoS_2-like structure, i.e. the Mo-Mo distance between nearest neighbors or a multiple of this structural distance. Likewise, if HYD sites are located exclusively on edges:

$$\mu_{iE} = \left(\frac{E_i}{l}\right)\sigma_i \qquad (8)$$

And if HYD sites can be found both on edges and rims:

$$\mu_{iER} = \left(\frac{E_i+R_i}{l}\right)\sigma_i \qquad (9)$$

Inserting equations (1) to (6) into (7) to (9) we obtain:

$$\mu_{iR} \sim \frac{2C}{N_i L_i} \qquad (10)$$

$$\mu_{iR_S} \sim \frac{C}{N_i L_i} \qquad (11)$$

$$\mu_{iE} \sim \frac{(N_i-2)C}{N_i L_i} \qquad (12)$$

$$\mu_{iER} \sim \frac{C}{L_i} \qquad (13)$$

$$\mu_{iER_S} \sim \frac{(N_i-1)C}{N_i L_i} \qquad (14)$$

Finally, since in general,

$$TOF_i = \frac{A_i}{\mu_i} \qquad (15)$$

where A_i is the HYD activity in molecule.g^{-1}.s^{-1}, and TOF_i the corresponding Turn Over Frequency in molecule.$site^{-1}$.s^{-1}. Equations (10) to (15) allow us to compare catalysts with the same Mo content, and shape factors for MoS_2-like nanoparticles. A_i , N_i, and L_i are provided by experiment, and can be used to assess if HYD sites are located on edges, rims, or both, since TOF_i should be the same in a family. Obviously, this model is an oversimplification of reality since M and S-edges are not distinguished, and possible stacking faults and defects are disregarded. Yet, provided that L and N values are statistically significant, it should capture trends and allow to discriminate situations in which active sites sit on rims only from situations in which they also sit on other edges. For supported catalysts, XRD will not

produce reliable estimates of L and N, since generally the highly dispersed MoS_2-like structures will remain undetectable due to the excessively broadened corresponding diffraction lines. The analysis should then be restricted to TEM results when available.

Table 1 : Rim-Edge model: test of data of Daage and Chianelli [14] – (a): k_{H4DBT} relative to catalyst MoS_2_340 °C ; (b) From Debye-Scherrer analysis of (100) XRD lines using Datathief and Fityk codes [16], matching the published value given for MoS_2-650 °C, (c) Standard Deviation, (d) Aspect Ratio AR = h(002)/L. All TOFs presented are relative and therefore dimensionless.

Catalyst	N	L	A (a)	TOF_{iR}	TOF_{iE}	TOF_{iRE}	NL^2	AR(d)
MoS_2_340°C	3.1	4.3	1.00	6.7	12.1	4.3	57.3	0.4
MoS_2_450°C	3.4	4.7	0.80	6.4	9.1	3.7	75.1	0.4
MoS_2_550°C	3.8	5	0.42	4.0	4.4	2.1	95.0	0.5
MoS_2_650°C	7.1	5.9 (b)	0.20	4.3	1.7	1.2	247	0.7
MoS_2_750°C	10.1	6.4 (b)	0.10	3.2	0.8	0.6	410	1.0
MoS_2_900°C	15.2	11.4	0.03	2.4	0.4	0.3	1990	0.8
			Mean	4.5	4.7	2.0		
			SD (c)	1.7	4.9	1.7		
			SD/Mean	0.4	1.0	0.8		

Let us start with the data of Daage and Chianelli, collected in Table 1. Our analysis based on XRD morphologies does identify the rim hypothesis as the most consistent hypothesis for this series of catalysts, since it produces the lowest relative standard deviation (SD/Mean) for TOF_{iR}. This agreement with the original analysis by Daage and Chianelli gives us confidence in our simplified approach, which we will now apply to two series of supported

catalysts with morphologies determined by TEM. The first series was published by Payen et al. [17], and its analysis is presented in Table 2.

Table 2: Rim-Edge model: test of data of Payen et al. [17] – (a): Activity for toluene hydrogenation relative to catalyst Mo-14 (14% MoO_3 supported on γ-Al_2O_3 in the calcined catalyst), (b): Co(Ni)Mo-3/14 (3% CoO and 14% MoO_3 supported on γ-Al_2O_3 in the calcined catalyst), (c): NiMoP-3/14/6 (3% NiO, 14% MoO_3, and 6% P_2O_5 supported on γ-Al_2O_3 in the calcined catalyst). (d): $\boldsymbol{TOF_{iR_S}}$ for the rim hypothesis in the case of supported catalyst**.** All TOFs presented are relative and therefore dimensionless.

Catalyst	N	L (nm)	A (a)	$\boldsymbol{TOF_{iR_S}}$	$\boldsymbol{TOF_{iRE}}$
Mo-14	1.4	3.5	1	4.9	3.5
CsMo-14	2.4	3.4	0.24	2.0	0.8
NaMo-14	1.8	3.8	0.96	6.6	3.6
FMo-14	2.7	3.3	1.46	13.0	4.8
CoMo-3/14 (b)	1.7	3.8	6.6	42.6	25.1
NiMo-3/14 (b)	1.5	4	12.5	75.0	50.0
NiMoP-3/14/6 (c)	2.3	2.7	13.8	85.7	37.3

This set of catalysts shows that additives (Cs, Na, F, P) and promoters (Co, Ni) have significantly more impact on the HYD activity than morphology. Alkaline elements act as inhibitors, while electronegative elements (F, P) act as boosters, as is well known. Besides, variations in N and L are limited on these supported catalysts. It is, however, reasonable to accept that HYD takes place on rim sites when comparing NiMo and NiMoP, for which TOF_{iRS} differ by less than 10%. In that case, introduction of P in the catalytic formula simultaneously increases A and affects the MoS_2-like nanoparticle morphology but at almost constant product NL and, thus, HYD active site density. P would then have a slight boosting effect on the HYD activity, reflected by the 10% increase of TOF_{iRS}. We will return to this point in section 3.

A third set of hydrogenation results was published by Fischer in his PhD Thesis [18]. Its analysis is presented in Table 3, which allows to examine the effect of F as a booster on Mo and NiMo catalysts supported on γ-Al_2O_3.

Table 3: Rim-Edge model: test of data of Fischer [18] – (a): Activity for ortho-xylene hydrogenation relative to catalyst Mo-12 (12% MoO_3 supported on γ-Al_2O_3 in the calcined catalyst), (b): NiMoF-3/13/3 (3% NiO, 14% MoO_3, and 3% F supported on γ-Al_2O_3 in the calcined catalyst). All TOFs presented are relative and therefore dimensionless. (c): Mean and Standard deviation for the three NiMoF catalysts.

Catalyst	N	L (nm)	A (a)	TOF_{iRS}	TOF_{iRE}	NL^2
Mo-12 (a)	1.7	4	1	6.8	4.0	27.2
FMo-12	2.0	4.3	1.4	12.0	6.0	37.0
NiMo-3/12	2.2	4.6	16.9	171	77.7	46.6
NiMoF-3/12/3 (b)	2.2	4.8	30	316.8	144.0	50.7
NiMoF-3/12/10	2.2	4.4	37	358.2	162.8	42.6
NiMoF-3/12/17	1.9	3.9	31.9	236.4	124.4	28.9
			Mean (c)	303.8	143.7	
			SD (c)	61.9	19.2	
			SD/Mean	0.20	0.13	

Table 3 shows similar promoting effects of adding F and Ni on supported Mo as Table 2. Adding 3% F to supported NiMo increases the HYD activity by a factor two, but the activity passes through a maximum as the fluorine content increases. NiMoF catalysts have

similar activities, while L decrease significantly as the F content increases, meaning that the active phase becomes more dispersed on the support, as the average nanoparticle volume NL^2 decreases by a factor 1.7. In those three cases, where the promoting effects of Ni and F on the HYD activity are similar, the best hypothesis is that active sites are located on both rims and edges, since TOF_{iRE} differ by less than 10 % while TOF_{iRS} scatter twice as much around the mean. However, the trend in TOFs passes through a maximum with increasing F content from 0 to 17% for both hypotheses. In other words, beyond some point the increased dispersion does not increase the activity. Comparing NiMo and NiMo+3%F, there is even a slight decrease in dispersion, while the HYD activity increases by a factor two. In that range, one must conclude that a direct or indirect electronic effect causes this secondary promotion by F.

Table 4 provides a similar analysis for a subset of unsupported NiMoS catalysts with exceptionally high HYD activity [19]. A multi technique characterization study showed that these solids could be described as fully decorated NiMoS nanoparticles supported on NiS or NiS_2. Very recently Lercher and coworkers [20, 21] obtained similar results for similar catalysts, prepared differently, and reported also a strong HYD selectivity with respect to DDS compared to NiMoS supported on γ-Al_2O_3. These authors used an elegant selective chemical etching method to eliminate nickel sulfides, leaving only NiMoS but eventually embedding NiS_x (where x remained undetermined). They did not discuss their results in terms of the rim-edge model. Inspection of Table 4 reveals that the rim hypothesis is less consistent than the rim+edge hypothesis, since the TOF_{iRE} values differ by less than 3% , and the TOF_{iR} values by 9%. For this set of catalysts, however, N, L, and A vary within a quite limited range.

Table 4: Rim-Edge model: test of data of Garreau et al. [19] – (a) : From Debye-Scherrer analysis of the (100) XRD lines using Datathief and Fityk codes [16] L in nm ; (b): Activity for toluene hydrogenation per g Mo relative to unsupported NiMoS (monophasic, $\alpha = (Ni/Ni+Mo)_{at.} = 0.25$); (c): industrial catalyst of first generation for reference; (d) Mean and SD for the NiMoS/NiS_x subset (x = 1 or 2); (e) TOF_{iRS}. All TOFs presented are relative and therefore dimensionless.

Catalyst	α	N(a)	L (a)	A (b)	TOF_{iR}	TOF_{iRE}
NiMoS	0.25	5.7	3.5	1	20.1	3.5
NiMoS/NiS_x	0.469	4.1	2.8	1.74	19.5	4.8
NiMoS/NiS_x	0.475	5.2	2.5	1.82	24.1	4.6
NiMoS/NiS_x	0.601	4.2	2.6	1.81	20.3	4.8
NiMoS/NiS_x	0.715	4.4	2.5	1.87	21.3	4.8
NiMoS/NiS_x	0.822	4.8	3.5	1.97	23.8	4.97
				Mean (d)	21.8	4.8
				SD (d)	2.0	0.13
				SD/Mean	0.093	0.028
NiMoS/γ-Al_2O_3(c)	0.3	1.5	3.5	1.15	3.0 (e)	3.98

It is worth noticing that the rim hypothesis cannot reconcile the TOFs of supported and unsupported NiMoS, while the rim+edge model can reconcile them. The effect of the NiS_x support on NiMoS results in an activity improvement by a factor two and 40% in TOF_{iRE}. Compared to NiMoS supported on γ-Al_2O_3 in the reference industrial catalyst of the first generation, the 60% activity improvement is significant, but not as much as reported by Lercher and coworkers (a factor 15) for the HYD pathway in HDS of DBT [20, 21]. The improvement in TOF_{iRE} is 14% only when NiMoS is supported on γ-Al_2O_3. One should of

course take into account that the preparation protocols of [19] and [20] were quite different. The origin of this peculiar HYD selectivity of NiMoS supported on NiSx is an open question.

« Brim edges » were termed by Topsøe and coworkers after their atom resolved observations, by Scanning Tunneling Microscopy (STM) in constant current topological mode, of continuous protrusions above the top basal planes of MoS_2 nanoparticles supported on Au(111) single crystals [22]. Such protrusions are localized along both Mo and S-edges. DFT calculations allowed to interpret these protrusions as signatures of one-dimensional metallic edge states, present on 100% S covered Mo-edges of triangular nanoparticles obtained under pure H_2S, as well as 50% SH covered S-edges of hexagonal nanoparticles obtained under H_2 + H_2S mixtures. The combination of STM experiments and DFT calculations later provided many other interesting results, like the observation of rapidly diffusing weakly-adsorbed thiolates in interaction with these brims, the localization of Co and Ni promoters decorating edges, and recently the observation of proton transfer to pyridine adsorbed on SH groups at CoMoS S-edges [23]. STM experiments cannot be performed on nanoparticles supported on insulating materials like γ-Al_2O_3 but the relevance of these model studies for HDS and HYD catalysis has been well supported by DFT studies. In between stacked nanosheets weakly bound by van der Waals forces, brim edges cannot be observed, but their existence cannot be ruled out.

Type I and II CoMoS structures were distinguished by Candia et al. [24] on the basis of higher TOFs for the latter, sulfided at 873 K, than the former sulfided at 673 K. This difference was attributed to the weaker interactions of the type II structures with the support, “when all Mo-O-Al linkages have been broken”, and assumed well modelled by single layer CoMoS structures on Au(111) exhibiting brim edges, as studied by STM. Sulfiding at higher temperature increases N (stacking), but decreases dispersion (increase L), so a preparation challenge was to prepare highly dispersed type II Co(Ni)MoS (lower L). As stated by Topsøe

et al. “The linkages can be broken by high temperature sulfiding but this decreases the MoS_2 edge dispersion and it is therefore preferable to find alternate procedures. This may occur by introduction of additives or chelating agents or by using weakly interacting supports” [25]. The BRIM™ family of catalysts, showing activities on real feedstocks improved by 15% to 20% both in HDS and HDN with respect to their previous generation of commercial catalysts, was introduced by Haldor Topsøe A/S as an undisclosed solution to this challenge. This corresponds for this company to a particular step in the staircase of increasing performances of competing commercial HDS catalysts, which may be seen as resulting from a kind of Darwinian evolutive process, partly guided by knowledge acquired from basic research efforts (see for instance Fig. 0.1 in [11]). This discussion shows that the brim edge phenomenon should be clearly distinguished from the rim-edge model, and from the BRIM trademark.

Baubet et al. [26] studied the influence of sulfidation conditions on the slab morphologies and properties of MoS_2/γ-Al_2O_3 model catalysts at constant Mo loading (8 wt % MoO_3). For catalysts sulfided in a flow of 15% H_2S in H_2 between 523 and 973 K, theory predicts hexagonal morphologies with 75 to 60% M-edges. Their TEM studies showed almost no variation of N in the temperature interval explored (~2.5), while L increased quasi linearly with temperature (squared regression coefficient R^2 = 0.935) between 2.8 and 4.1 nm. HYD and HDS catalytic activities were evaluated simultaneously in a batch reactor for a mixture of 2,3-dimethylbut-2-ene (23DMB) (10 wt.%), and 3-methylthiophene (3MT) (0.3 wt.%) dissolved in n-heptane. Normalizing the reported activities by the reported Mo^{4+} contents (as measured by XPS) allows to compute relative activities and TOFs according to the simple model presented in the foregoing. These relative activities increased linearly with increasing 1/L (R^2= 0.995 and 0.976 for HYD and HDS respectively), while the selectivity HDS/HYD remained almost constant until 673 K then decreased. Since N is almost constant it is not possible to discriminate between the rim model (TOF_{iRS}) and the rim+edges (TOF_{iRE}) models,

but for the latter, calculated HYD turn-over frequencies deviate less than 8% from the average. This study addressing the hydrogenation of an olefin rather than an aromatic brings therefore a complementary information.

The study of Baubet et al. also includes a comparison with catalysts sulfided under pure H_2S, predicted to exhibit 100% M-edges (triangular nanoparticles), with similar results, except for less regular increase of L with sulfidation temperature. The HDS/HYD selectivities were strictly correlated between both series ($R^2 = 0.997$), and higher by 18% for the 100% M-edge cases. They fall below one for high sulfidation temperatures (from 823 K onward). Assuming that relative activities measured for the 15% H_2S in H_2 series are a linear combination of contributions of M-edges and S-edges, and that the 100 % H_2S series provides the activities intrinsic to the M-edges, it is possible to calculate HDS and HYD TOFs for S-edges: While HDS TOF seems almost constant with increasing sulfiding temperature up to 673 K, then decreases sharply, the HYD TOF seem to pass through a minimum value at 623 K, so that their ratio is maximal around this sulfidation temperature. According to the Type I/Type II concept, one would expect to find systematically higher TOFs both for HYD and HDS for sulfidation temperatures higher than 623K. From the above analysis of the results of Baubet et al., this would be the case only for HYD on S-edges. These authors rightfully underlined their observation of a much sharper decrease of the specific activity in HDS than the amount of exposed edges, which remains to be explained. However, this cannot be compared to the results of Candia et al., which were relative to CoMoS structures, for which the transition above 623 K is likely to involve complex processes like a redistribution of Co atoms between M and S-edges, and changes of S coverages for both edges.

More recently, Baubet et al [27] showed that a shape index obtained by an advanced statistical analysis of high-resolution scanning transmission electron microscopy in high-angle annular dark field mode (HR HAADF-STEM) images of CoMoS nanolayers supported on γ-

Al_2O_3 is correlated with the measured HDS/HYD selectivity. Thus, they confirm the higher HDS selectivity of Co-promoted S-edges over Co-promoted M-edges under the same catalytic conditions as the previously mentioned study. They convincingly invoke DFT result by Krebs et al [28] to explain this difference on the basis of higher affinity ratios 3MT/23DMD on Co-promoted S-edges than on Co-promoted M-edges. They obtain a marked increase of HDS activity per edge site for sulfiding temperatures under pure H_2S between 623 K and 900 K, compatible with the type II concept, i.e well sulfided nanolayers in weak interaction with the support. Both HDS and HYD activities drop drastically, however, beyond 973 K, but this is outside the range of realistic sulfiding conditions. Notice that the practical challenge in these studies was the selective HDS of gasoline produced by Fluid Catalytic Cracking (FCC), avoiding as far as possible the loss of octane index caused by hydrogenation of olefins. In contrast, rather different catalysts are used for pretreating feedstocks for FCC or hydrocracking, processes for which the goal is to maximize hydrogen transfer by hydrogenation of polyaromatics and hydrodenitrogenation (HDN), which go on a par, while maintaining high levels of HDS.

One conclusion of this section is that for supported catalysts, similar to those used in industrial practice, the validity of the rim-edge model is questionable. In the case of unsupported MoS_2 it explains the results. However, one can also expect that as the nanoparticle volume NL^2 and aspect-ratio AR increase as the annealing temperature increases (cf. Table 1), attractive van der Waals forces will tend to increase the edge-to-edge or basal plane-to-edge interparticle sticking probabilities with respect to basal plane-to-basal plane sticking (faulted stacking). Interparticle sticking will then hinder or shadow more and more edge sites in a way indistinguishable by XRD, as long as sticking does not mean sintering. This effect would be difficult to discriminate from what the rim-edge model describes. It will be much less probable for catalysts supported on γ-Al_2O_3 or titania, in which the basal planes

of Co(Ni)MoS nanocrystallites interact strongly with the support surfaces [29, 30] and tend to remain well dispersed and isolated.

Bekx-Schürmann et al. reported recently the effect of reduction temperature under H_2+He mixtures on the morphology, the chemisorption of O_2, CO and N_2O and on the ethene hydrogenation activity of unsupported MoS_2 [31]. The conditions of preparation and catalysis are rather remote from practical hydrotreating. These authors conclude from the better correlation obtained with ethene HYD activity that CO is the most reliable probe for coordinatively unsaturated sites. XRD and TEM analysis revealed that L and N did not change significantly as reduction temperature is raised until 673 K. At 873K however, there was a marked increase of N and L, and broadening of their distributions (from TEM statistics). As expected, a simple morphological model similar to the one presented here cannot reconcile all measured properties since the growth of nanocrystalline MoS_2 under H_2 at 873 K induces anisotropic stacking, i.e. exposing basal planes preferentially to edge planes, and does not heal defects. The authors conclude that HYD activity originates from brim states: However, their results are also consistent with the remark made above on Daage and Chianelli results, that an over expression of basal planes for high aspect-ratio 100/001 MoS_2 crystallites at the fluid-solid interface might artificially shadow edge sites.

3 HYD activity of supported NiMoS doped with B, P, and F

Primary and secondary promoters have a dominant effect on HYD activity. While the effect of primary promoters (Co, Ni) is rather well explained by the volcano plot as discussed in the Inroduction, the action of secondary promoters or inhibitors is still debated (see for instance [32]) and rational guidelines are missing. In this section, the well-known doping effect of the electronegative elements P, B, and F on HYD activity of γ-Al_2O_3 supported

NiMoS will be considered from a new point of view, and a unifying interpretation of its origin tentatively proposed.

Table 5 presents the properties of a set of γ-Al_2O_3 supported NiMo catalysts incorporating various amounts of P, B, and F, including combinations of these elements. Details on the preparation and characterization protocols can be found in Supplementary Materials. Figures 2 and 3 present the main results, which can be extracted from Table 5. For all catalysts, the HYD TOF (TOFa) appears to be correlated to a single descriptor, the atomic ratio β = (P+B+F)/Ni (Fig. 2). The correlation holds up to β ~ 9, which corresponds to the simultaneous presence of P, B, and F in the catalyst. Since in the same test, isomerization of cyclohexane to methyl-cyclopentane occurs, catalyzed by Brønsted acid sites (BAS), it provides an acidity scale for this set of catalysts. Isomerization proceeds trough a bifunctional mechanism, involving first cyclohexane dehydrogenation to cyclohexene on a hydrogenation/dehydrogenation site, then proton transfer from BAS to the olefin and isomerization of the resulting adsorbed carbocation. Considering that the dehydrogenation step is required and rate limiting, isomerization rate constants were normalized by the amount of chemisorbed CO like HYD rate constants, in order to estimate Turn Over Numbers for isomerization (TOFb).

Two linear correlations appear between TOFb and the atomic ratio β in Fig. 3, one for catalysts resulting from the addition of P, B, and F to the NiMo catalyst A, and the other for catalysts resulting for the additions of B and F to the NiMoP catalyst B. In the latter case, P was introduced simultaneously with Ni and Mo in a single incipient wetness impregnation step, so that one might expect that it interacts differently with the other hard anion-forming elements than added *a posteriori* to A. For catalysts based on A, TOFb remains low, weakly dependent of the amount of doping element, whereas for catalysts based on B a significant isomerization activity develops with increasing doping.

Notice that the NiMoP catalyst considered in Table 2 exhibits only a modest 10% increase in HYD activity compared to its NiMo counterpart, while with similar P/Ni ratios, catalyst B is 60% more active than its counterpart A (Table 5). This illustrates the well-known importance of preparation and testing on the catalytic properties of formulae with apparently identical elemental analysis. As a consequence, as was done here, comparisons should be performed for series of catalysts as far as possible homogenous regarding experimental protocols followed, or for different sets when they include a common reference.

From a chemical standpoint, the question arises therefore to what extent do P, B, and F behave analogously in the strong sulfo-reducing environment of the catalytic tests, having been introduced as the hard anions PO_4^{3-}, BO_3^{3-}, and F^-. Ferdous et al. [33] showed that the K-edge XANES of the elements P and B introduced into a NiMo/γ-Al_2O_3 catalyst imply that these elements remain coordinated by oxygen after sufidation and several days on stream in hydroprocessing conditions. Sun et al. [34] extensively reviewed and discussed also the effect of P and F on hydrotreating catalysts, and established a parallel with the effect of chelating agents, both acting as hard basic ligands. They concluded that the improved HYD activity was due to the weakened interaction of Ni(Co)MoS phases with the supports easing sulfidation, decoration by the promoter, and formation of the type II phases [24], i.e. stacked (higher N). Bonduelle and Guichard reported that addition of complexing agents to Ni and Co delay the sulfidation of these promoters (ref [11] page 205). Therefore “easing sulfidation” might refer to a thermodynamic rather than kinetic effect. Type II is assumed beneficial for aromatics hydrogenation compared to type I, which is defined as single sheets of Co(Ni)MoS in stronger interaction with the support (N=1). Notice that this conjecture is opposite to the rim-edge model, which implies inactive edge sites, but consistent with the compilations presented in Tables 1 to 4. The result shown in Fig. 2 holds, however, for HYD activities per site (TOF), i.e. independent from the MoS_2-like nanoparticle morphology, as far as CO chemisorption can

be accepted as titrating active sites (S vacancies) of hydrotreating catalyst, as shown by Bachelier et al. [35]. Until recently, others have explained the improved HYD activity of supported NiMoS catalysts doped by hard anion-forming elements as a dual effect induced by the increased Brønsted acidity [32]. However, since the comparison of Figs. 2 and 3 shows that TOFa and TOFb are not correlated, one must exclude the existence of a causal relationship between acidity and HYD, although isomerization needs both functions. In contrast, one may conclude that an electronic effect of the increased concentration of hard basic anions in the catalysts, irrespective of their nature, is the main cause of the improved HYD activity. If this is the case, other questions arise: Can hard anions in strong interaction with the support induce this electronic effect indirectly at relatively long range, or are doping elements present, in part, on the NiMoS phase? And in the latter case, in which chemical state?

Fischer has shown [18] that increased F doping of a NiMo/γ-Al_2O_3 catalyst from 0 to 4 wt % resulted in an increase from 43 to 47% of the Cis/(Cis+Trans) ratio ρ of the 1,2-dimethylcyclohexane isomers produced in a o-xylene HYD test. He found hardly any change for a F-doped unpromoted Mo/γ-Al_2O_3 catalyst up to 7 wt% F, ρ staying close to 53%. As long as ρ remains kinetically determined in this catalytic test, it is known to be indicative of the ratio of "flat" adsorption of o-xylene (i.e. η6) on the catalyst surface to "side on" (i.e. η1), higher ρ being determined by a more favorable free energy of adsorption. Furthermore, in ref. [36] Fischer et al. interpreted a higher ρ as indicative of a higher electronic density localized on the active sites. This suggests that the electronic effect of hard anions on the NiMoS phase is to slightly increase the strength of the "flat" adsorption, also described by the metal-sulfur bond energy E_{MS}, so that on the volcano curve described by the latter quantity, the points of the doped catalysts are shifted to the right. Since undoped NiMo is located on the left-hand side of the volcano (lower E_{MS} than optimal), doped NiMo would come closer to the optimum,

which can be located at a slightly lower E_{MS} than NiW (see for instance Fig. 1.11 in [11]). According to this hypothesis one should observe an adverse effect of hard anions on the HYD activity of CoMo catalysts, which lie on the right-hand side (higher E_{MS} than optimal) slope of the volcano. This is however not the case (see for instance [37], showing improved HDN activity on a real feedstock, indicative of HYD, for CoMoP with respect to CoMo).

Rather, let us consider that since H_2S is neither a reactant nor a product in the hydrogenation of aromatics, but merely a competitor for molecular or dissociative adsorption on sulfur vacancies, the heats of reaction and scaling relationships for reactants and products are independent of its partial pressure. Therefore, according to our recent result [3], the descriptors E_{MS} of the optimal catalysts for these reactions in a sulfo-reductive reaction medium should not change, while the activities may change, so that the whole volcanoes may be shifted upwards or downwards, while abscissae stay fixed, as depicted in the Table of Contents Graphic and Supplementary Materials Figure S2. Moreover, one may expect that hard anions repel H_2S, for instance through relatively long range opposite dipole-dipole interactions, either as bound to the support and forming BAS, or in part adsorbed on Ni(Co)MoS edge vacancies. Analogously to fluorination of solid surfaces, which brings hydrophobicity, we would observe in the present case what could be termed as sulfhydrophobicity. In other words, the effect of adding hard anions to sulfided hydrogenation catalysts would be to impart more thioresistance, in analogy with the known effect of halogen adsorption on noble metal hydrogenation catalysts [38]. This might be verified by simple comparative kinetic experiments varying the partial pressure of H_2S imposed in the reactor. As shown in Supplementary Materials, the measured apparent order with respect to H_2S for toluene hydrogenation is -0.2 ± 0.03 over the NiMoP catalyst (B in Table 5). This should be compared to the value of -0.34 reported by Guernalec et al. (see Fig. 3 in [39]) for NiMo (similar to catalyst A in Table 5). The NiMoP catalyst is therefore less inhibited by H_2S.

Chen et al. [40] studied the effect of B addition up to 1.8 wt % on the properties of a γ-Al_2O_3 support and of the corresponding MoS_2/γ-Al_2O_3 and CoMoS/γ-Al_2O_3 catalysts (15.5 % MoO_3, Co/(Co+Mo)=0.3. With increasing B addition, they found in particular a linear increase of BAS as quantified by integration of the the band at 1654 cm^{-1} of adsorbed 2,6-dimethylpyridine. L and N were almost constant for both types of sulfided catalysts, as revealed by statistical analysis of TEM images. They observed a systematic linear or almost linear increase of TOFs for the HYD routes in 2,6-dimethyldibenzothiophene HDS, and 2,6-dimethylaniline HDN. Moreover, they reported linear relationships between adsorbed CO stretching frequencies for bands assigned to adsorption on Mo and Co coordinatively unsaturated sites (CUS) at edges of the sulfide phases, and boron content. The red shifts of both bands decreased simultaneously by about 2.8 $cm^{-}1$ per wt % B added to the support. Chen et al. concluded that "the electronic deficiency character of the MoS_2 and CoMoS sites increases with boron loading in agreement with the trends observed on pure Mo sulfide phase". However, it is now well recognized that frequency shifts of vibrational modes of adsorbed CO manifest a vibrational Stark effect [41, 42], i.e. the interaction of the local electric field with the molecule dipole moment. Rather intricated charge transfers affecting this dipole moment are expected between adsorbed CO and the various coordinatively unsaturated surface sites of MoS_2 and CoMoS involving d-bands. This is probably why Travert et al. [43] could not find correlations between DFT computed CO adsorption energies and frequency shifts for relevant MoS_2, CoMoS, and NiMoS atomistic models of edge sites. In the absence of evidence or chemical indication that B can be incorporated in MoS_2 or CoMoS nanoparticles, it is reasonable to assume that its presence does not interfere with donations and back donations affecting the dipole moment of adsorbed CO. Rather, each hard anion and Brönsted base BO_3^{3-}, HBO_3^{2-} and $H_2BO_3^{-}$ formed in interaction with the alumina support surface (e.g. sharing O^{2-} ions with Al^{3+} ions), will be a negatively charged source,

either a point charge, or a dipole if neutralized by protons, contributing more or less strongly to a background electrostatic potential opposed to that generated by coordinatively unsaturated Mo and Co cations. Therefore, one expects CO molecules to probe increasingly attenuated local electric fields in presence of increasing surface concentrations of B (and other hard anions forming elements). According to the physics of the vibrational Stark effect, the frequency shift with respect to the isolated molecule should be proportional to the local field at constant dipole moment. In summary, the linearly decreasing red shift with increasing boria coverage observed by Chen et al. can be interpreted as a consequence of this electrostatic interaction.

For a system which does not involve transition metals, Toulhoat et al. [44] have recently shown by a combination of DFT calculations and experiments, that absolute values of frequency shifts for CO adsorbed on various edge and basal planes surface sites of nanotalc ($Si_4O_{10}Mg_3(OH)_2$) are roughly correlated with the corresponding adsorption energies, and blue shifts and red shifts linearly correlate with the respectively negative (shortened) or positive (lengthened) relative changes of equilibrium C-O bond lengths of adsorbed molecules. If this result can be transposed to the present case of supported sulfides nanoparticles, it would mean that the effect of boron described by Chen et al. can be interpreted as *decreasing* the adsorption energy of CO on the coordinatively unsaturated sites of interest, at constant charge transfers. These sites would remain characterized by unchanged covalent M-S bond energies E_{MS}. Molecular adsorption of H_2S on the same sites also involve charge transfers and for a significant part the energy of this process is expected to be correlated to E_{MS}. But H_2S is a polar molecule, the adsorption of which is also influenced by the local electrostatic field. Therefore, its molecular adsorption should also be electrostatically weakened in the vicinity of hard anions, in favor of non-polar aromatic molecules competing for adsorption on the same sites, and in agreement with the less negative apparent order of

HYD with respect to H_2S partial pressure mentioned above (-0.2 for NiMoP compared to -0.34 for NiMo). This would rationalize the favorable unspecific doping effect of hard anions, or "sulfhydrophobic effect". Checking this interpretation would of course necessitate an extensive study combining experiments and theoretical calculations, beyond the scope of the present Perspective.

Table 5 : Properties of γ-Al_2O_3 supported NiMo doped by electronegative elements. (a) atomic ratio Ni/(Ni+Mo); (b) atomic ratio; (c) First order rate constant for toluene HYD normalized by Ni atom, in millimole toluene per mole Ni per second; (d) mole CO per mole Ni; (e) Turn Over Frequency in h^{-1} (TOFa = k_{HYD}/CO); (f) First order rate constant for cyclohexane isomerization normalized by Ni atom, in millimole cyclohexane per mole Ni per second; (g) Turn Over Frequency in h^{-1} (TOFb = k_{is}/CO); (h) active elements in the calcined catalyst Mo 9.3 wt %, Ni 2.36 wt %; (i) active elements in the calcined catalyst Mo 10.4 wt%, Ni 2.12 wt%, P 2.61 wt %.

Catalyst	α (a)	P/Ni (b)	F/Ni (b)	B/Ni (b)	(P+B+F)/Ni (b)	k_{HYD} (c)	CO (d)	TOFa (e)	k_{is} (f)	TOFb (g)
A (NiMo) (h)	0.29	0.00	0.00	0.00	0.00	2.85	0.104	99	0.11	3.7
A+H_3BO3	0.31	0.00	0.00	1.25	1.25	2.95	0.062	171	0.16	9.2
A+$(NH_4)_3PO_4$	0.31	7.72	0.00	0.00	7.72	2.70	0.035	276	0.10	10.4
A+NH_4F	0.31	0.00	2.81	0.00	2.81	2.61	0.045	207	0.09	7.2
A+ HBF_4	0.29	0.00	2.21	0.34	2.55	4.76	0.100	171	0.29	10.4
B (NiMoP) (i)	0.25	4.82	0.00	0.00	4.82	4.65	0.075	222	0.11	5.1
B+H_3BO_3	0.24	4.76	0.00	1.03	5.79	6.06	0.073	298	0.29	14.3
B+HBF_4	0.23	4.84	3.41	0.63	8.88	4.49	0.048	335	0.76	56.5

4 Conclusions

Three strategies generally considered for improving the selectivity of Ni(Co)MoS phases towards hydrogenation of aromatics and polyaromatic hydrocarbons were discussed: i) maximising rims, ii) maximising stacking, and iii) doping with hard anion-forming elements (e.g; P, B, F). Improved hydrogenation is desirable for upgrading heavy cuts into clean fuels, and well-known to be in particular the key to improve hydrodenitrogenation (HDN) upstream of hydrocracking or Fluid Catalytic Cracking.

Simple geometrical considerations show that the so-called rim-edge model, which applies well for unsupported MoS_2 nanocrystallites of variable aspect-ratio (stacking number N and diameter L of MoS_2-like layers), is not consistent with trends observed for NiMoS catalysts supported on γ-Al_2O_3 or NiSx , were active sites would rather lie on rims as well as edges. Increased shadowing of edge sites by edge-to-edge and edge-to-base nanoparticle interactions, with increased edge over bases areas, might as well explain the results reported for unsupported MoS_2 nanocrystallites of variable aspect-ratio.

An increased dispersion of the NiMoS phases is favorable for HYD activity, meaning that L should be minimized. Increased N will ensue if the number of active nanoparticles per unit area of support is conserved, but is not critical.

Doping supported NiMoS by hard anion-forming elements affects dispersion (i.e. L and N) by modifications of the support surface properties, but more significantly unspecifically increases the TOF of active sites for hydrogenation, leaving unchanged the periodic trend described by the metal-sulfur bond energy E_{MS}. This phenomenon may be explained by an increased "sulfhydrophobicity", due to repulsive interactions between H_2S and adsorbed hard anions at the gas-solid interface, thus favoring aromatics in the competition for covering edge sulfur vacancies. This concept is illustrated by Fig. S2 in Supplementary Materials, and in the Table of Contents Graphic. Further experimental and theoretical work will be necessary in order to check this interpretation. It is also well known that such doping creates acid sites in γ-Al_2O_3 supported Ni(Co)MoS catalysts, but it is shown that they cannot be the cause of the general increase of HYD TOF.

NiSx supported NiMoS catalysts exhibit a significantly improved HYD activity compared to unsupported NiMoS, and γ-Al_2O_3 supported NiMoS. The reconsideration of the results of Garreau et al. [19] in terms of TOF_{iRE} supports their conclusions on a more

quantitative basis, and allows a comparison to some extent with the recent results of Lercher et al. ([20], [21]). However, it does not allow to fully understand the origin of these improvements. It remains therefore also another interesting open question, both for theory and experiments.

Acknowledgement:

This paper is dedicated to the memory of Henrik Topsøe, for his inspiring and outstanding contributions to understanding structure and functions of catalysts.

I am grateful to IFP Energies nouvelles for 36 years of an extremely stimulating career, and permission to publish the present results.

I am indebted to Roel Prins for his helpful suggestions to improve the style and organization of this Perspective.

References

[1] H. Topsøe, B.S. Clausen, R. Candia, C. Wivel, S. Mørup, J. Catal., 68 (1981) 433.

[2] B.E. Stangeland, Industrial & Engineering Chemistry Process Design and Development 13, 1 (1974), 71.

[3] H. Toulhoat, P. Raybaud, Catalysis Science & Technology, 10, 7, (2020), 2069.

[4] P. Sabatier, Berichte der Deutschen Chemischen Gesellschaft 44 (1911) 1984.

[5] A.A. Balandin, in Advances in Catalysis, W. G. Frankenburg, V. I. Komarewsky, D. D. Eley and P. B. Weisz, (Eds) Academic Press, New York, 1958, vol. 10, p. 96

[6] S.J. Trasatti, Electroanal. Chem. 39 (1972) 163.

[7] C.J.H. Jacobsen, S. Dahl, B.S. Clausen, S. Bahn, A. Logadottir, J.K. Nørskov, J. Am. Chem. Soc. 123 (2001) 8404.

[8] H. Toulhoat, P. Raybaud, J. Catal. 216 (2003) 63.

[9] J.K. Nørskov, T. Bligaard, J. Rossmeisl, C.H. Christensen, Nat. Chem. 1 (2009) 37.

[10] S. Kasztelan, H. Toulhoat, J. Grimblot, J.P. Bonnelle, Appl. Catal. 13 (1984) 127.

[11] H. Toulhoat and P. Raybaud (Eds), Catalysis by Transition Metal Sulfides, from Molecular Theory to Industrial Application, Editions Technip, Paris, 2013.

[12] C. Thomazeau, C. Geantet, M. Lacroix, M. Danot, V. Harlé, P. Raybaud, Appl. Catal. A 322 (2007) 92.

[13] J. Kibsgaard, A. Tuxen, K.G. Knudsen, M. Brorson, H. Topsøe, E. Laesgsgaard, J.V. Lauritsen, F. Besenbacher, J. Catal. 272 (2010) 195.

[14] M. Daage, R.R. Chianelli, J. Catal. 149 (1994) 414.

[15] S. Cristol, J. F. Paul, E. Payen, D. Bougeard, F. Hutschka, S. Clémendot , J. Catal. 224 (2004) 138.

[16] https://datathief.org and https://fityk.nieto.pl

[17] E. Payen, R. Hubaut, S. Kasztelan, O. Poulet, J. Grimblot, J. Catal. 147 (1994) 123.

[18] L. Fischer, PhD Thesis, University of Paris 6, 1999.

[19] F.B. Garreau, H. Toulhoat, S. Kasztelan, R. Paulus, Polyhedron 5 (1986) 211.

[20] M. F. Wagenhofer, H. Shi, O.Y. Gutiérrez, A. Jentys, J. A. Lercher, Sci. Adv. 6 (2020) eaax5331.

[21] F. Vogelgsang, Y. Ji, H. Shi, J. A. Lercher, J. Catal. 391 (2020) 212.

[22] V. Lauritsen, M. Nyberg, J.K. Nørskov, B.S. Clausen, H. Topsøe, E. Lægsgaard, F. Besenbacher , J. Catal. 224 (2004) 94.

[23] S. S. Grønborg, N. Salazar, A. Bruix, J. Rodríguez-Fernández , S. D. Thomsen, B. Hammer, J. V. Lauritsen, Nature Commun., 9 (2018) 2211.

[24] R. Candia, O. Sorensen, J. Villadsen, N.Y. Topsøe, B.S. Clausen, H. Topsøe, Bull. Soc. Chim. Belg., 93 (1984) 763.

[25] H.Topsøe, R. G. Egeberg, K. G. Knudsen , Prepr. Pap. Am. Chem. Soc., Div. Fuel Chem. 49 (2004), 2, 568.

[26] B.Baubet, E. Devers, A. Hugon, E.Leclerc, P. Afanasiev, Appl. Catal. A 487 (2014) 72.

[27] B. Baubet, M. Girleanu, A.-S. Gay, A.-L. Taleb, M. Moreaud, F. Wahl, V. Delattre, E. Devers, A.Hugon, O. Ersen, P. Afanasiev, P. Raybaud, ACS Catal. 6 (2016) 1081.

[28] E. Krebs, B. Silvi, A. Daudin, P. Raybaud, J. Catal. 260 (2008) 276.

[29] C. Arrouvel, M. Breysse, H. Toulhoat, P. Raybaud, J. Catal. 232 (2005) 161.

[30] D. Costa, C. Arrouvel, M. Breysse, H. Toulhoat, P. Raybaud, J. Catal. 246 (2007) 325.

[31] S. Bekx-Schürmann, S. Mangelsen, P. Breuninger, H. Antonia, U. Schürmann, L. Kienle, M. Muhler, W. Bensch, W. Grünert, Appl. Catal. B, 266 (2020) 118623.

[32] W. Han, H. Nie, X. Long, M. Li, Q. Yang, D. Li, Catal. Today 292 (2017) 58.

[33] D. Ferdous, A.K. Dalai, J. Adjaye, J. Mol. Cat. A, 234 (2005) 169.

[34] M. Sun, D. Nicosia, R. Prins, Catal. Today 86 (2003) 173.

[35] J. Bachelier, M. J. Tilliette, J. C. Duchet, D. Cornet, J. Catal. 76 (1982) 300.

[36] L. Fischer, V. Harlé, S. Kasztelan, Stud. Surf. Sci. Catal. 127 (1999) 261.

[37] H. Toulhoat H., J.P. Poitevin, I. Igniatiadis, Actes du 2eme Colloque Franco-Vénézuélien de Catalyse, IFP, E, 22-26/04/85, 1985. And https://www.osti.gov/etdeweb/servlets/purl/20671899 Figure 12 page 34.

[38] P.A. Gravil, H. Toulhoat, Surf. Sci. 430 (1999) 192.

[39] N. Guernalec, C. Geantet, T. Cseri, M. Vrinat, H. Toulhoat, P. Raybaud , Dalton Trans., 39 (2010) 8420.

[40] W. Chen, F. Maugé, J. van Gestel , H. Nie , D. Li , X. Long, J. Catal. 304 (2013) 47.

[41] S.D. Fried, S. G. Boxer, Acc. Chem. Res. 48 (2015) 998.

[42] F. Leydier, C. Chizallet, D.Costa, P. Raybaud, Chem. Commun. 48 (2012) 48, 4076.

[43] A. Travert, C. Dujardin, F. Maugé, E. Veilly, S. Cristol, J.-F. Paul, E. Payen, J. Phys. Chem. B 110 (2006) 1261.

[44] H. Toulhoat, L. Lin, D. Brouri, J.-M. Krafft, Y. Millot, G. Laugel, H. Lauron-Pernot, J. Phys. Chem. C 123 (2019) 26965.

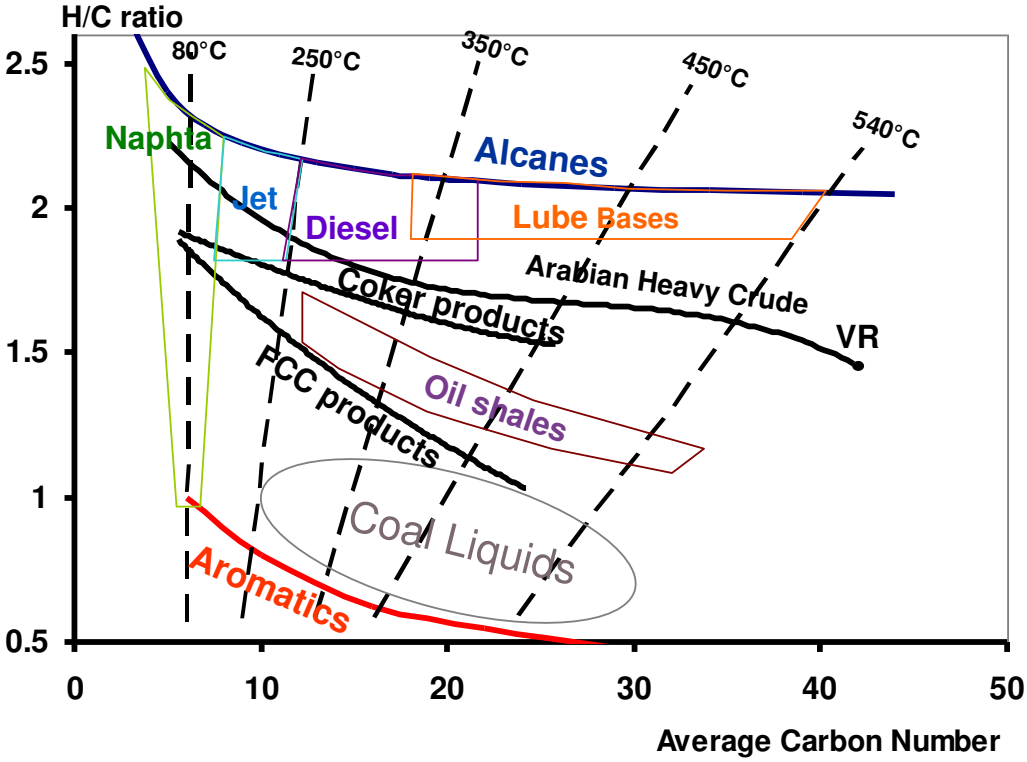

Figure 1: The "Stangeland diagram" showing the necessity of increasing the H/C for upgrading fossil feedstocks to fuel grade products. VR: Vacuum Residue. Dotted lines are iso-boiling points.

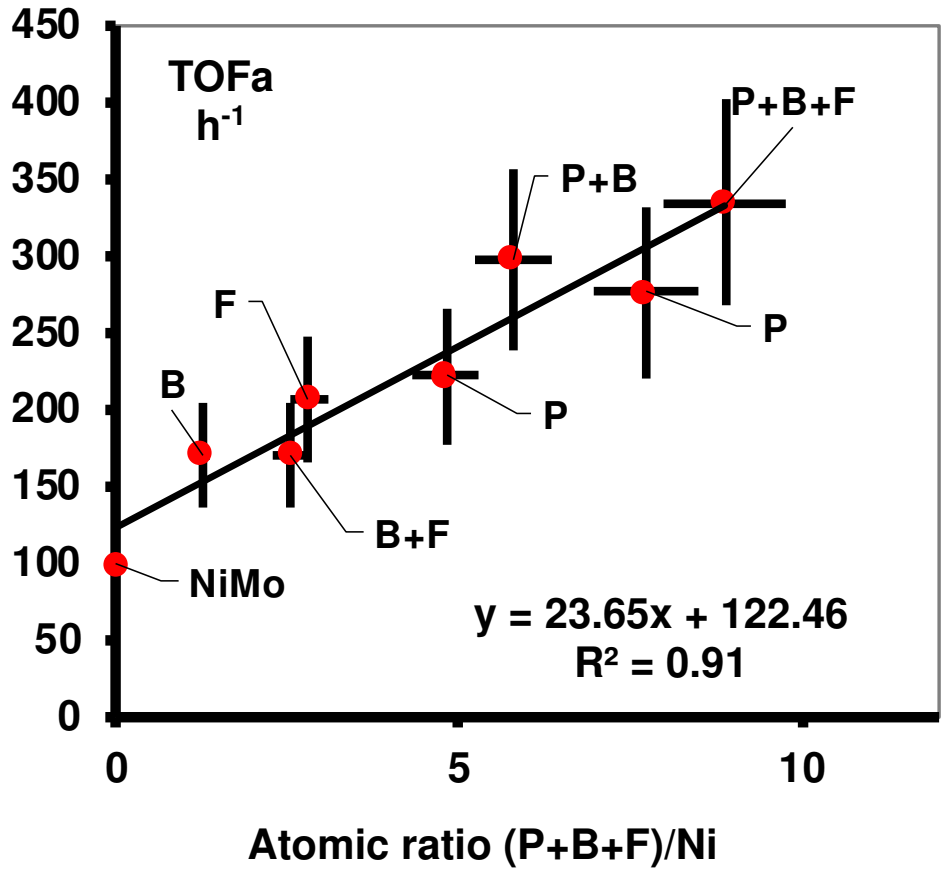

Figure 2: Correlation between Turn Over Frequency for toluene hydrogenation (TOFa = kHYD/CO) in presence of H_2S and concentration of hard anions forming elements in a NiMo/γ-Al_2O_3 catalyst (data from Table 5). Error bars: 20% in ordinates, 10% in abscissae (from estimation of accuracies of experimental measurements from which the data are derived).

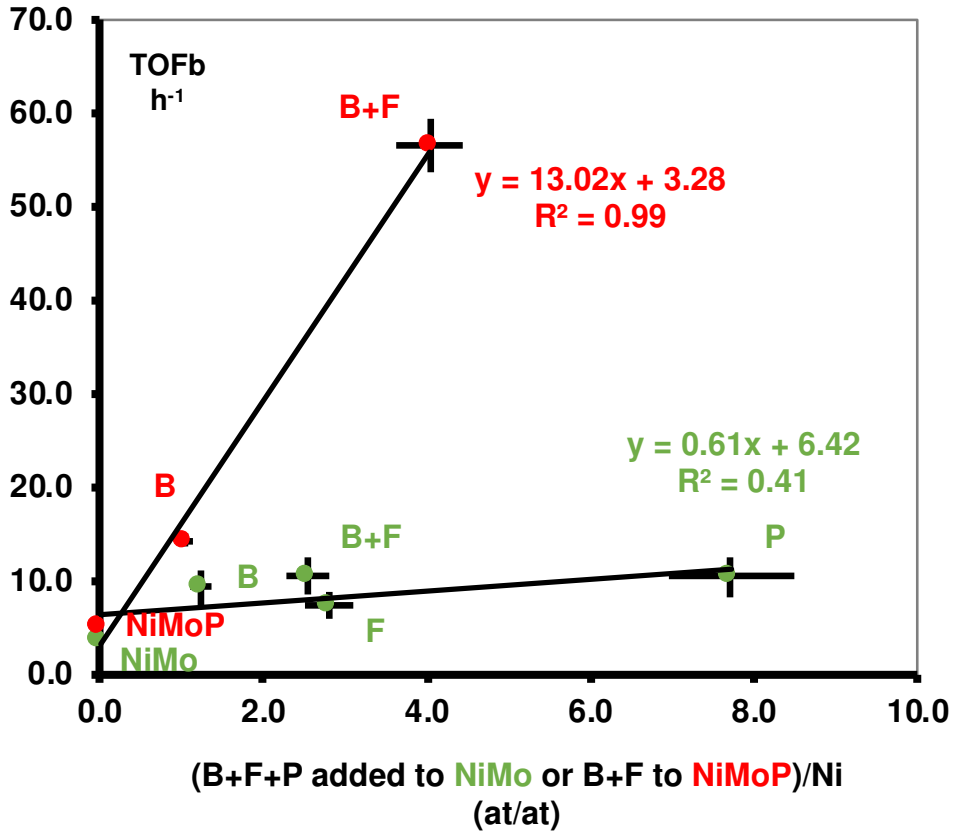

Figure 3: Correlation between Turn Over Frequency for isomerization of cyclohexane (TOFb = kis/CO) in presence of H_2S and concentration of hard anions forming elements added in a NiMo/γ-Al_2O_3 catalyst, green dots, or a NiMoP/γ-Al_2O_3, red dots (data from Table 5). Error bars: 20% in ordinates, 10% in abscissae (from estimation of accuracies of experimental measurements from which the data are derived).

TOC Graphic

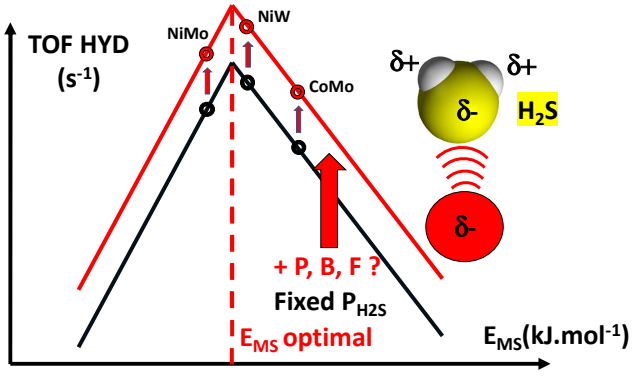
TOF HYD
(s-1)
NiMo
NiW
CoMo
δ+
δ+
δ-
H2S
δ-
+ P, B, F ?
Fixed PH2S
EMS optimal
EMS(kJ.mol-1)